

CONCLUSION

The basic mechanisms of transfluxor operation have been shown and a few examples given on how this versatile component may be used.

The multiload transfluxor is constructed by placing additional reading apertures in the core and wiring each hole for separate addressing. This permits many read operations to take place throughout the memory at the same time. Each readout is delivered to its own independent load. The nondestructive read property eliminates the rewrite time associated with conventional

core memories; this feature permits cutting the read time in half.

It appears that, by utilizing these properties, considerably more flexibility and speed can be built into a transfluxor memory. The independent operation of the various parts of the memory would facilitate communication between sections of a computer or between two computers and would permit all parts of a computer network to operate without delays due to memory time-sharing. This would be a major advance in computer design.

Design and Analysis of MAD Transfer Circuitry*

D. R. BENNION† AND H. D. CRANE†

I. INTRODUCTION

THIS is the second in a series of papers¹ concerned with a technique for performing combinatorial and sequential digital logic with magnetic elements and connecting wires only. These elements are termed MAD's (Multi-Aperture Devices). For clarity, in the first paper the basic techniques were described in terms of simple circuit structures which do not represent the best that can be achieved in the way of operational properties. The object of this paper is: 1) to present circuit techniques for significantly improving the circuit operation; and 2) to present experimental and analytic results which are pertinent to an understanding of the coupling loop operation.

The basic coupling loop and clock cycle are briefly reviewed in the next section.

II. REVIEW OF BASIC COUPLING LOOP AND CLOCK CYCLE

The circuits discussed here use only POSITIVE MAD elements¹ (although the results are applicable to circuits using other types of MAD elements). Each element has at least two small apertures, one used for an output winding and one for an input winding. The output winding of one element connects with the input winding of another to form a coupling loop, and in this way a pair of electrically connected elements is formed. As information is shifted along a chain of elements, each

element alternately plays the role of a receiver and transmitter.

Output Aperture

An element can be in either the Set (binary *one*) or Clear (binary *zero*) state, Fig. 1. Typical ϕ_T - F_T (where F_T is the driving mmf $N_T I_T$) curves for the output aperture of a transmitter for these two states are illustrated in Fig. 1(c). If the element is in the Set state, Fig. 1(b), then flux changes locally about the output aperture in response to small values of mmf F_T , whereas if the element is in the Clear state, Fig. 1(a), flux can change only about a path enclosing both the output and central apertures. Because of the longer path length in the latter case, larger switching mmfs are required. (Subscript T indicates that this winding is connected with the transmitter end of a coupling loop.)

Input Aperture

A receiver element is always cleared to its *zero* state before transmission into it. It operates then only along a ϕ_R - F_R Clear curve (where F_R is the mmf $N_R I_R$) which is essentially the same as the Clear-state curve for the transmitter, since the relevant path lengths are the same, Fig. 2(a) and 2(b).

An important property of a system in which windings connect with apertures, as indicated here, is that once an element is Set, it is impossible to Clear it from any aperture winding. In Fig. 2(c), an element is shown Set, as a result of current I_R . In Fig. 2(d), the same element is shown after a subsequent "negative set" current, $-I_R$. Note that as a result of the negative set current flux changes only *locally* about the input aperture *without* disturbing the flux about the output aperture.

* This work was carried out at the Stanford Research Inst., Menlo Park, Calif., under the sponsorship of the Burroughs Corp. Res. Center, Paoli, Pa.

† Stanford Res. Inst., Menlo Park, Calif.

¹ H. D. Crane, "A high-speed logic system using magnetic elements and connecting wire only," Proc. IRE, vol. 47, pp. 63-73; January, 1959.



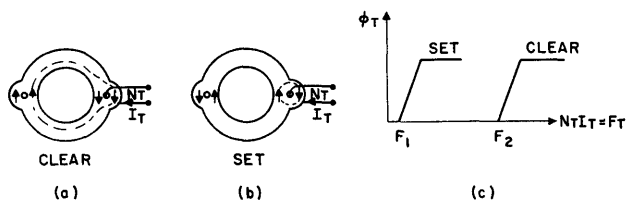


Fig. 1—Output aperture properties.

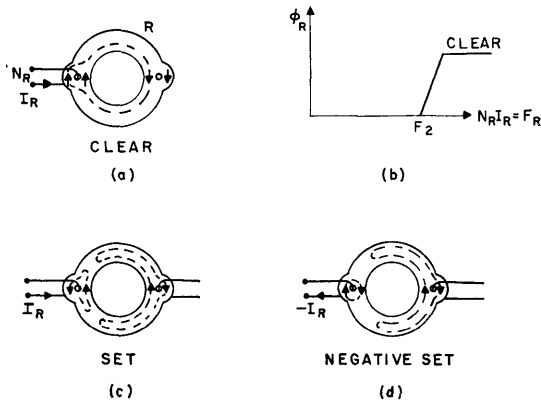


Fig. 2—Input aperture properties.

Coupling Loop

To form a coupling loop, the output winding of one element is connected to the input winding of the next (Fig. 3). If the transmitter is in the *zero* state, then transmission is trivial in the sense that the receiver is already in the *zero* (reference) state. It is necessary then that the Advance current I_A be controlled in value so that in this case no flux switches in either element. With the transmitter in the *one* state, it is desirable that I_R (and hence I_A) be as large as possible to facilitate flux transfer. For best transmission then, it is desirable to make I_A as large as allowable. The largest allowable value I_A is determined by the *zero* state condition, and is equal to

$$I_A^m = I_T^m + I_R^m = \frac{F_2}{N_T} + \frac{F_2}{N_R}$$

where F_2 is the Clear-state threshold mmf (Figs. 1 and 2). In this case, assuming that the current divides into $I_T = F_2/N_T$, and $I_R = F_2/N_R$, both devices are brought just to their thresholds F_2 , but no flux is switched. Thus a *zero* is "transmitted" as a *zero*. If the transmitter is in the Set state, however, the transmitter has a much lower threshold, F_1 , so that $I_R \gg I_T$ and the Advance current I_A causes flux switching in both the transmitter and the receiver. Thus the receiver is set to the *one* state.

Clock Cycle

A clock cycle for operating a two-MAD-per-bit shift register is briefly reviewed, Fig. 4. The elements are considered in two groups, arbitrarily labelled O (odd)

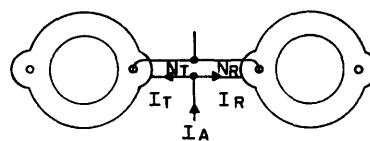


Fig. 3—Basic coupling loop.

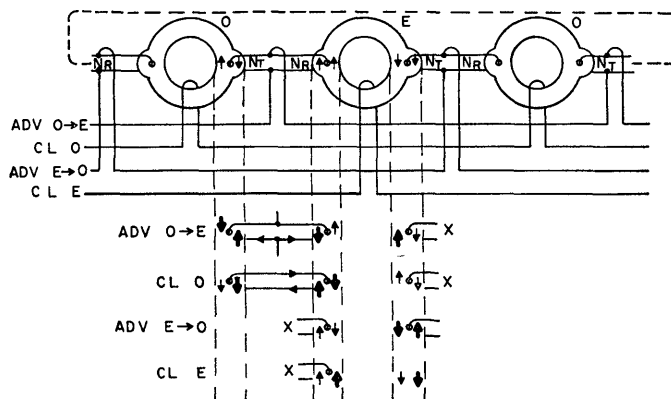


Fig. 4—Clock cycle.

and E (even). Information is stored in one group while the other is being cleared. The information is then shifted to the cleared group, while the other group is cleared, etc.

To get started in the cycle, assume the data are initially stored in the O elements. The ADV O→E pulse shifts the information to the E elements. The O elements are then explicitly cleared by the CL O pulse. The ADV E→O pulse shifts the information back to the O elements, and the E elements are then cleared by the CL E signal, etc. Thus the basic cycle is

$$\dots, \text{ADV O} \rightarrow \text{E}, \text{CL O}, \text{ADV E} \rightarrow \text{O}, \text{CL E}, \dots$$

By tracing the details of the data transmission, one may see how the MAD elements and basic clock cycle work together to yield unilateral transmission. As previously indicated, transmission of a *zero* is trivial. Transfer of a *one* is followed in detail in Fig. 4. The statements made with reference to this particular *one* transfer are true as well for every O→E loop simultaneously transferring a *one*.

Flux switched in any leg as a result of a particular pulse is indicated by a heavy arrow. The ADV O→E pulse switches flux locally about the output aperture of the O element and causes the E element to be set. The CL O pulse then clears the O element and in so doing switches flux through the output winding. This results in a loop current flow that negatively sets [see Fig. 2(d)] the E element (receiver) *without* affecting the flux state about the output aperture of the E element. Note that neither the ADV O→E nor CL O pulse causes any flux to be switched in the output leg of the E element (indicated by the crosses opposite the output winding), eliminating thereby the need for the conventional series coupling diode. ADVANCE E→O shifts the binary *one*

to the next O element in the direction of transmission, and CL E then clears the E element. Note again that neither the ADV E→O nor CL E pulses cause any flux to be switched in the input winding of the E element, eliminating the need for the conventional shunt diode to prevent backward transmission. Thus unilateral data flow is achieved.

Unity Turns Ratio Operation

Coupling loops can be successfully operated under conditions where $N_T \geq N_R$. The condition $N_T = N_R$ is particularly interesting for shift register circuits since the coupling loops are inherently symmetrical, and shifting may therefore be made to occur in either direction by control of the clock sequencing. Furthermore, the special case $N_T = N_R = 1$ results in very simple mechanical assemblies. The condition $N_T < N_R$ does not appear to have any particular advantage, but the condition $N_T > N_R$ is important as a means for obtaining flux gain when bi-directional coupling loops are not required. Operation with unity-turns-ratio, *i.e.*, $N_T = N_R$, is discussed in Sections V and VII.

In order to simplify the mathematical relations all circuit descriptions will be for symmetrical unity-turns-ratio coupling loops. The extension to the more general case $N_T > N_R$ is relatively straightforward.

Advance Current Range

It is well known that magnetic circuits that operate in the region of threshold are inherently slower and less tolerant to clock current variations than would be similar circuits not so limited. It is important therefore to determine and to take advantage, insofar as possible, of all techniques for improving these allowable operating ranges.

Relations for advance current range are derived below for the coupling loop circuit of Fig. 3, using a very simple model in which we assume 1) that the *one*, *zero* ϕ_T - F_T curves have vertical steps at threshold F_1 and F_2 (Fig. 5); 2) that if a transmitter element is in the *zero* state, then the circuit must be limited so that as a result of the Advance pulse, the receiver is not brought over its Clear state threshold F_2 ; and 3) that if the transmitter is in the *one* state, then as a result of the Advance pulse, the receiver element and transmitter element are completely switched. For this latter condition, the receiver must receive a net drive of at least F_2 and the transmitter a net drive of at least F_1 . Although this model is extremely inadequate (see Sections VII and VIII), it is very useful for comparative estimating purposes.

For the circuit of Fig. 5(a), the maximum value of Advance current I_A^{\max} is determined by the *zero* transfer condition. In this case, $I_A^{\max} = 2(F_2/N)$ where F_2/N is the current required in each branch to just bring its corresponding element to its Clear state mmf threshold F_2 .

The minimum value of Advance current, I_A^{\min} , is de-

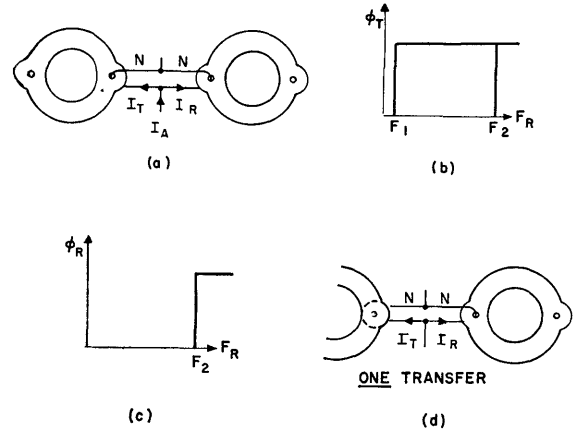


Fig. 5—Switching model for basic coupling loop.

termined by the *one* transfer condition. The equivalent circuit of Fig. 5(d) can best be used for visualizing the relations, so that

$$I_A^{\min} = I_T^{\min} + I_R^{\min} = \frac{F_1}{N} + \frac{F_2}{N}.$$

Therefore, the percentage range R for the Advance current, defined as

$$R = \frac{(I_A^{\max} - I_A^{\min}) \times 100}{I_A^{\text{av}}}$$

is equal to

$$R = 2 \left[\frac{F_2 - F_1}{3F_2 + F_1} \right] \times 100. \quad (1)$$

For comparative purposes, it is interesting to consider the limiting case when $F_1 = 0$. Under these conditions, the limiting value of range, R^0 , is

$$R^0 = 67 \text{ per cent.} \quad (1a)$$

In the sections to follow, circuits that exhibit significantly greater range will be introduced and the expressions for range determined for these may be compared with the relation derived here.

It may be noted that in these circuits only the Advance current range is of concern since the Clear current range is essentially unlimited, as long as it is above the minimum value required for adequate clearing of the elements.

Switching Speed

It is well known that the rate of switching of a "square loop" magnetic material is approximately proportional to the amount of (excess) drive, over and above the threshold value. Thus, two thin rings (of the same material) of radii r_1 and r_2 would switch at the same rate if driven with mmf's in the ratio r_1/r_2 .

For the switching problem at hand, we will estimate the switching speed with the Advance current set in the

TABLE I
SUMMARY OF RANGE AND SPEED RELATIONS DERIVED IN TEXT

Figure	Condition	R [Range in fraction of 100 per cent]	R^0 [R for $F_1 = 0$]	Number of switching thresholds n measured at I_A^{av}	$n^0 - 1$ (n^0 is value for $F_1 = 0$)
5		$2 \left(\frac{F_2 - F_1}{3F_2 + F_1} \right)$	$\frac{2}{3}$	$\frac{3F_2 + F_1}{2(F_1 + F_2)}$	$\frac{1}{2}$
9	let $F_2^B = F_2 + F_B$	$2 \left(\frac{F_2^B - F_1}{3F_2^B + F_1} \right)$	$\frac{2}{3}$	$\frac{3F_2 + F_B + F_1}{2(F_1 + F_2)}$	$\frac{1}{2} \left(\frac{F_2^B}{F_B} \right)$
10	$N \geq 4N_B$ $N \leq 4N_B$ $N = 4N_B$	$2 \left[\frac{(F_2 - F_1)N + 2F_1N_B}{(3F_2 + F_1)N - (4F_2 + 2F_1)N_B} \right]$ $2 \left[\frac{F_2N - (2F_2 + F_1)N_B}{F_2N + F_1N_B} \right]$ $2 \left[\frac{2F_2 - F_1}{4F_2 + F_1} \right]$	$\frac{2N}{3N - 4N_B}$ $\frac{2(N - 2N_B)}{N}$ 1	$\left[\frac{(3F_2 + F_1)N - (4F_2 + 2F_1)N_B}{2(F_1 + F_2)(N - 2N_B)} \right]$ $\left[\frac{F_2N + F_1N_B}{2(F_1 + F_2)N_B} \right]$ $\left[\frac{4F_2 + F_1}{2(F_1 + F_2)} \right]$	$\frac{N}{2(N - 2N_B)}$ $\frac{N - 2N_B}{2N_B}$ 1
11	$F_{dc} \geq \left(\frac{4N_B}{N} - 1 \right) F_2$ $F_{dc} \leq \left(\frac{4N_B}{N} - 1 \right) F_2$ $F_{dc} = \left(\frac{4N_B}{N} - 1 \right) F_2$ $N = 2N_B$ and $F_{dc} = F_2$	$2 \left[\frac{(F_2 - F_{dc} - F_1)N + 2F_1N_B}{(3F_2 - 3F_{dc} + F_1)N - (4F_2 - 4F_{dc} + 2F_1)N_B} \right]$ $2 \left[\frac{(F_2 + F_{dc})N - (2F_2 + F_1)N_B}{(F_2 + F_{dc})N + (F_1 - 2F_{dc})N_B} \right]$ $2 \left[\frac{2F_2 - F_1}{4F_2 - 2F_{dc} + F_1} \right]$ $2 \left[\frac{2F_2 - F_1}{2F_2 + F_1} \right]$	$\frac{2N}{3N - 4N_B}$ $2 \left[\frac{(F_2 + F_{dc})N - 2F_2N_B}{(F_2 + F_{dc})N - 2F_{dc}N_B} \right]$ $\frac{2F_2}{2F_2 - F_{dc}}$ 2	$\left[\frac{(3F_2 - F_{dc} + F_1)N - (4F_2 + 2F_1)N_B}{2(F_1 + F_2)(N - 2N_B)} \right]$ $\frac{(F_2 + F_{dc})N + F_1N_B}{2(F_1 + F_2)N_B}$ $\left[\frac{4F_2 + F_1}{2(F_1 + F_2)} \right]$ $\left[\frac{4F_2 + F_1}{2(F_1 + F_2)} \right]$	$\frac{(F_2 - F_{dc})N}{2F_2(N - 2N_B)}$ $\frac{N(F_2 + F_{dc})}{2N_B F_2} - 1$ 1 1
12	Relations same as in Fig. 10 with N replaced by $N' + 2N_B'$ and N_B replaced by N_B'				
13	Relations same as in Fig. 10 with N replaced by $2(N_1 + N_2)$ and N_B replaced by N_1				

middle of its calculated range, *i.e.*, with the Advance current set at

$$I_A^{\text{av}} \left(\text{that is, } \frac{I_A^{\text{max}} + I_A^{\text{min}}}{2} \right).$$

With the transmitter and receiver windings directly in parallel, then at every instant during the switching process,

$$N_T \frac{d\phi_T}{dt} = N_R \frac{d\phi_R}{dt}$$

where ϕ_T and ϕ_R are the switched fluxes in the T and R elements, respectively. With equal turns, $N_T = N_R$, the branch currents will divide so as to cause the same number of thresholds, n , in the transmitter and receiver. This will result in equal switching rates, *i.e.*, $\dot{\phi}_T = \dot{\phi}_R$. Furthermore, according to the ϕ - NI model of Fig. 5, I_T and I_R will be constant during the switching process (see Fig. 23). The number of thresholds in the transmitter is equal to $n_t = NI_T^{\text{av}}/F_1$ and in the receiver is equal to $n_r = NI_R^{\text{av}}/F_2$ where $I_T^{\text{av}} + I_R^{\text{av}} = I_A^{\text{av}}$. By setting $n_t = n_r = n$, then we find the relation

$$n = \frac{3F_2 + F_1}{2(F_2 + F_1)}. \quad (2)$$

In the limiting case, $F_1 = 0$, then

$$n^0 = 1.5 \text{ thresholds.} \quad (2a)$$

This value of n^0 could easily have been predicted by noting that

$$I_A^{\text{av}} = \frac{3F_2}{2N}.$$

For the ideal case assumed here, during *one* transfer, the entire Advance current flows into the receiver. Thus, $n^0 = NI_A^{\text{av}}/F_2$.

The relations for range, for n , and for switching speed proportional to $n-1$ derived here are listed in Table I, along with corresponding relations for the circuits derived below. (It should be kept in mind that speed, $1/\tau$, where τ is switching time, is proportional to the *excess* number of thresholds of drive and hence $n-1$, since n was defined as the total number of thresholds.)

Motivation

It is clear from the above relations for R and n that one way to improve the speed and advance current range is to make F_2 large relative to F_1 . This implies the use of a large diameter element, compared to the diameter of the small aperture. However, a large element is undesirable for many obvious reasons. It is fortunate, though, that the equivalent of a large element can be obtained by appropriate biasing arrangements. But even further, the biasing arrangements can improve the operation even beyond what would be expected merely of a "larger" element.

Another way to improve the speed, and in general the range as well, is to provide as much drive as possible about the output aperture of the transmitter. Under the ideal condition of threshold $F_1 = 0$, then it requires no current to switch the transmitter, and $I_R = I_A$ during *one* transmission. This is equivalent to saying that all of the mmf appearing about the transmitter output aperture in the *zero* state is transferred to the receiver via the coupling loop during *one* transmission.

Consider again the elementary coupling loop of Fig. 6 with I_A^{max} applied, Fig. 6(a) and 6(b). During *zero* transfer, both the transmitter and receiver are stressed with a threshold mmf F_2 . During *one* transfer, at least ideally, the receiver becomes stressed by $2F_2$. If appropriate circuitry can provide higher stresses in the transmitter (around the output aperture) during *zero* transfer, then the receiver stress during *one* transmission is correspondingly higher. Generally, this can be achieved in two ways, Fig. 6(c) and 6(d). In Fig. 6(c), the coupling loop applies an mmf of $2F_2$, which ordinarily would tend to set a *zero* transmitter. However, this is prevented by a bias equal to F_2 so that the net setting mmf about the central aperture in the *zero* state is still only F_2 . Furthermore, the bias F_2 is not strong enough to clear a set transmitter during *one* transfer. Thus, with this arrangement, a stress of $2F_2$ can be added to the receiver during *one* transfer, resulting in a total receiver stress of $3F_2$.

In the arrangement of Fig. 6(d), a *zero* state stress of $2F_2$ is also achieved in the transmitter, but this is obtained by applying an extra clear direction drive of magnitude F_2 on the inner leg.

Alternate schemes combining these approaches may be used as well, as indicated in Fig. 6(e), where k , which may have any value, but practically will lie in the range $1 \leq k \leq 2$, is an arbitrary constant. In this case, the net stress about the output aperture is $2F_2$, independent of k . Note that the circuit of Fig. 6(c) results from $k=2$, and the circuit of Fig. 6(d) for $k=1$.

The initial circuit arrangements that follow are motivated from these concepts. However, as these circuits develop other concepts arise which lead to still other circuits.

III. SCHEMES UTILIZING ONLY A SINGLE WINDING IN THE INPUT AND OUTPUT APERTURES

Transmitter Bias

With a current I_{BT} in the clear direction through a winding of N_{BT} turns linking the central aperture of the transmitter (Fig. 7), the Advance mmf $N_T I_T$ must first overcome the mmf $F_{BT} = N_{BT} I_{BT}$ before it can switch flux about the central aperture of the transmitter. This "bias," therefore, effectively increases the magnitude of the threshold F_2 by the value F_{BT} . The equivalent threshold is, therefore, $F_2' = F_2 + F_{BT}$. The threshold F_1 is not affected, however, since the bias current does not link the flux paths that are local about the output aperture. Thus, to the electrical circuit the element ap-

pears to be larger than it actually is. The magnitude of bias is limited to a value $N_{BT}I_{BT} = F_2$ or the bias mmf itself would tend to clear a Set transmitter. Thus, with maximum bias, $F_{BT} = F_2$, the element appears to be twice as large in diameter, and the effective threshold F_2' is essentially twice F_2 .

Receiver Bias

With the transmitter in the *zero* state, the manner in which I_A initially tends to divide between transmitter and receiver branches depends upon the branch inductances L_T and L_R , which are attributable mainly to the saturation permeability of the ferrite. However, the final division of current depends only on branch wire resistances R_T and R_R . For identical elements and with turns ratio N_T/N_R , the ratio of branch inductances is $(N_T/N_R)^2$. It is desirable to make the resistance ratio the same in order to eliminate transient overshoots in the branch currents. At the same time, it is desirable for R_T/R_R to be in the ratio N_T/N_R (in the case of no transmitter bias) in order for the final mmf's applied to transmitter and receiver to be equal. The above two conditions appear to be incompatible for $N_T/N_R \neq 1$ or even for $N_T/N_R = 1$ if transmitter bias is being used. However, by application of bias $N_{BR}I_{BR}$ to the receiver (Fig. 8), an additional term is added to the receiver mmf and the above conditions can both be satisfied. In this sense then, receiver bias serves as a free parameter for simultaneous satisfaction of one additional loop condition.

For the case $N_T = N_R = N$, it is clear that receiver bias should be equal to transmitter bias for proper balance. At the same time, this leads to a symmetrical loop capable of bidirectional transmission.

It is important to note that whereas the transmitter bias must be limited to, at most, the value F_2 , the receiver bias can be of arbitrary value. This is so because the receiver current can only cause flux switching about the central aperture of the receiver, and the only concern, therefore, is with the net mmf $(N_R I_R - N_{BR} I_{BR})$ about the central aperture. During *one* transmission any flux switching about the central aperture of the transmitter in the Clear direction is detrimental.

Simultaneous Transmitter and Receiver Bias

With bias $F_B = F_{BT} = F_{BR}$ applied, the maximum value of I_A^{max} is [Fig. 9(a)]

$$I_A^{max} = \frac{2(F_2 + F_B)}{N} = \frac{2F_2^B}{N}$$

where $F_2^B = F_2 + F_B$, and from Fig. 9(b), I_A^{min} is

$$I_A^{min} = \frac{F_1}{N} + \frac{F_2 + B}{N} = \frac{F_2^B + F_1}{N}$$

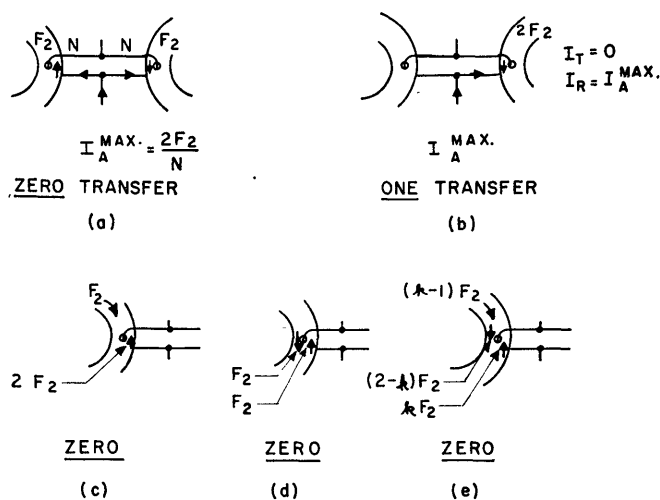


Fig. 6—Basic biasing arrangements.

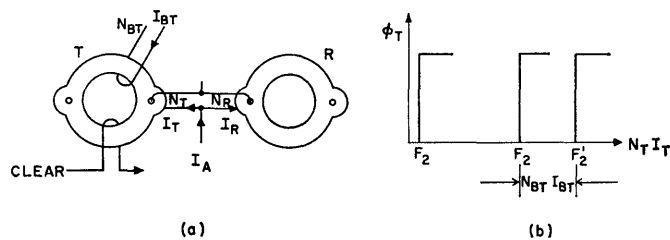


Fig. 7—Transmitter bias.

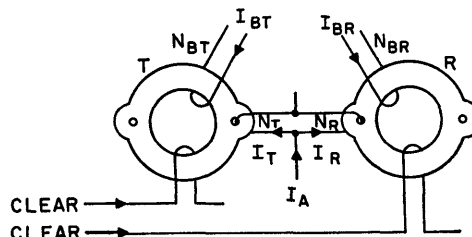


Fig. 8—Receiver bias.

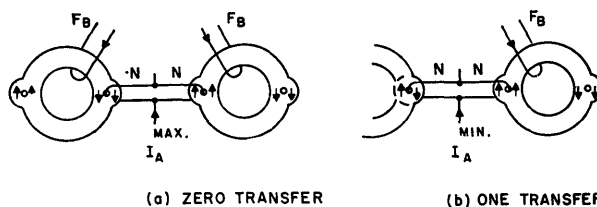


Fig. 9—Circuit using separate transmitter and receiver bias.

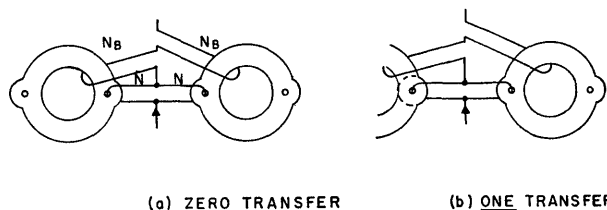


Fig. 10—Circuit using compatible transmitter and receiver bias.

Therefore, the range R is

$$R_{SB} = 2 \left[\frac{F_2^B - F_1}{3F_2^B + F_1} \right] \times 100 \quad (3)$$

and, again for the limiting case $F_1 = 0$,

$$R_{SB}^0 = 67 \text{ per cent} \quad (3a) \quad \text{or}$$

where the subscript SB implies that this range is for circuit with simple bias. The switching factor n can be found in the same way as for (2); thus,

$$n_{SB} = \frac{NI_{T^{av}}}{F_1} = \frac{NI_{R^{av}} - F_B}{F_2} = \frac{3F_2 + F_B + F_1}{2(F_2 + F_1)} \quad (4)$$

and

$$n_{SB}^0 = 1.5 + \frac{F_B}{2F_2}. \quad (4a)$$

It is interesting to note that with bias mmf F_B applied, the range is increased exactly as though F_2 were replaced by a larger element of dimension $F_2^B = F_2 + F_B$. However, the switching speed is improved beyond just the simple substitution of F_2^B for F_2 in (2).

Thus, by the use of bias in this manner, the switching properties are significantly improved. This bias could be provided from a dc source, or from a pulse source. In the next section, it is indicated that still further advantage is obtained by having the bias mmf provided by the Advance current itself.

Compatible Bias

In order to keep the number of current sources to a minimum and also to insure that the receiver bias operates only during the Advance current (if, by design, it should be greater than F_2), it is desirable to have the Advance current itself provide the bias as indicated in Fig. 10.

In this circuit arrangement, there are two conditions for I_A^{\max} . For $N \geq 4N_B$, then I_A^{\max} is limited by the *zero* transfer, in which case

$$I_A^{\max} = \left[\frac{F_2 + N_B I_A^{\max}}{N} \right]_T + \left[\frac{F_2 + N_B I_A^{\max}}{N} \right]_R$$

or

$$I_A^{\max} = \frac{2F_2}{N - 2N_B}.$$

If I_A^{\max} were larger than this value, then the transmitter and receiver would overrun their threshold during *zero* transfer.

For $N \leq 4N_B$, then I_A^{\max} is limited by the *one* transfer, in which case

$$I_A^{\max} = \frac{F_2}{N_B}.$$

For values larger than this, the transmitter would tend to be cleared during transfer. In either case, I_A^{\min} is determined from Fig. 10(b), where

$$I_A^{\min} = \left[\frac{F_1}{N} \right]_T + \left[F_2 + N_B I_A^{\min} \right]_R$$

$$I_A^{\min} = \frac{F_2 + F_1}{N - N_B}.$$

The resulting relations for R_{CB} , n_{CB} , R_{CB}^0 , and n_{CB}^0 are given in Table I, where the subscripts CB imply the compatible bias use. Note that R_{CB} and n_{CB} are functions of N and N_B . Of course, with $N_B = 0$ these relations reduce to the same relations as given in (1) and (2).

Maximum R_{CB}^0 and n_{CB}^0 occur for $N = 4N_B$ in which case

$$R_{CB}^0 = 100 \text{ per cent} \quad (5)$$

$$n_{CB}^0 = 2. \quad (6)$$

The increased range obtained with compatible bias can be explained in terms of "moving thresholds." That is, with compatible bias, the effective transmitter threshold ($F_2 + N_B I_A$) is itself a function of I_A . Hence, as I_A increases from the center of its range and, therefore, tends to approach the threshold F_2 , the effective threshold value itself tends to increase, reducing considerably the overrunning effect. The same stabilization results in the case of Advance current reduction as well, as far as the receiver is concerned. Thus, as I_A decreases from the center of its range, the receiver moves further from threshold, but the effective threshold itself is decreasing. Note that with $N = 4N_B$, and with I_A^{\max} applied, the circuit of Fig. 10 exactly matches the conditions of Fig. 6(c).

Thus, significant improvement in R and n is obtained by the use of compatible bias. However, in practical circuits, N is greater than N_B , and since the minimum value of N_B is unity, single turn coupling loops cannot effectively be used.

Counter Bias

In order to improve the stabilization and, therefore, increase the Advance current range still further, it is necessary to increase the feedback effect; *i.e.*, it is necessary to make the bias "move" even faster as a function of Advance current. This may be achieved by increasing the bias turns N_B relative to the coupling loop turns N . However, for a given value of I_A and N , as the bias turns are increased the transmitter bias increases, and soon overruns 100 per cent. This effect may be compensated for by use of a dc bias of opposite sign (*i.e.*, counter bias), as indicated in Fig. 11.

As in the previous case there are two conditions for I_A^{\max} . For the case where $F_{dc} \geq ((4N_B/N) - 1)F_2$, then I_A^{\max} is determined from the *one* transfer case.

$$I_A^{\max} = \left. \frac{F_2 + N_B I_A^{\max} - F_{dc}}{N} \right]_T + \left. \frac{F_2 + N_B I_A^{\max} - F_{dc}}{N} \right]_R$$

or

$$I_A^{\max} = \frac{2(F_2 - F_{dc})}{N + 2N_B}.$$

The minimum current I_A^{\min} is determined for *one* transfer and is

$$I_A^{\min} = \left. \frac{F_1}{N} \right]_T + \left. \frac{F_2 + N_B I_A^{\min} - F_{dc}}{N} \right]_R$$

or

$$I_A^{\min} = \frac{F_2 - F_{dc} + F_1}{N - N_B}.$$

These combine into the relations for R_{dc} and n_{dc} given in the table.

For the alternate condition $F_{dc} \leq (4N_B/N - 1)F_2$, then I_A^{\max} is given simply from the *one* transfer case as

$$I_A^{\max} = \frac{F_2 + F_{dc}}{N_B}.$$

The relation for I_A^{\min} is the same as before.

The range is a maximum where $F_{dc} = ((4N_B/N) - 1)F_2$. Nominally, the dc bias is limited in magnitude to the value of F_2 . For this value of dc bias maximum range occurs for $N/N_B = 2$, and is equal to 200 per cent. The corresponding value of switching factor is $n^0 = 2$. Thus, ultimately, a 2 to 1 improvement in operating range is achieved.

This improvement in operating range is obtained at the expense of an extra dc bias. However, no extra windings are required since the dc current may be simply carried on the existing Clear windings. Furthermore, although range improvement is obtained at the expense of a new current source, dc currents are very simply regulated compared with pulse currents. Finally, the magnitude of the dc counter-bias current may be used as a fine control to aid in achieving the optimum operating point.

IV. MULTIPLE WINDINGS IN INPUT AND OUTPUT APERTURES

The circuits discussed thus far have all employed only a single winding in the input and output apertures. By relaxing this restriction, significant advantages can be obtained.

Drive on Inner Output Leg

With low-turn windings in the coupling loops, the Advance currents can become relatively large. By using the drive scheme indicated in Fig. 12, then for the same number of coupling loop turns, the advantages of com-

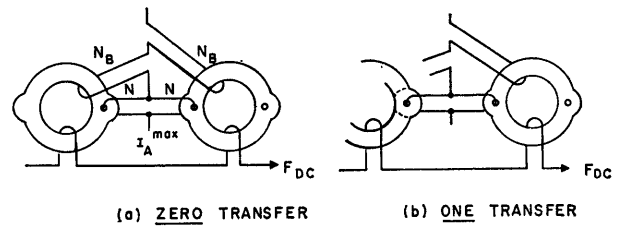


Fig. 11—Circuit using dc counter bias.

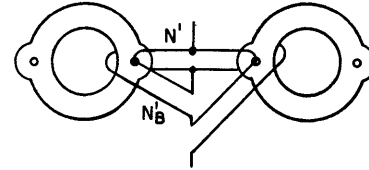


Fig. 12—Circuit using inner-leg drive.

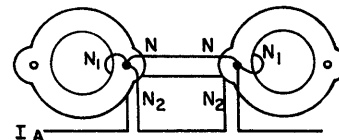


Fig. 13—Circuit using floating coupling loop.

patible bias can be obtained but with significantly lower Advance currents. In this circuit the Advance current is made to link the inner leg about the output aperture of the transmitter, as well as the coupling loop itself.

The equations for this case are identical to the equations for compatible bias if in the latter equations N is replaced by $(N' + 2N_B')$ and N_B by N_B' . Thus, for example, the case $N' = 3$, $N_B' = 1$ with the present scheme is identical to $N = 5$, $N_B = 1$ in the earlier scheme. Thus, $N' = 2$, $N_B' = 1$ yields maximum range corresponding to the case $N = 4$, $N_B = 1$, which was shown to be optimum for the earlier scheme.

Although, for a given number of coupling loop turns, there are more total turns in the small aperture, the additional drive turns may be of relatively small wire, since the main concern is only to make the coupling loop turns as large as possible to reduce coupling loop resistive losses.

Floating Coupling Loop

The circuits discussed thus far have the following two disadvantages: 1) with the coupling loop directly driven, care has to be exercised in physically connecting the two branch windings together so that proper ratios of the (parasitic) resistance and inductance are maintained and 2) since the same advance current flows through the coupling loops and bias windings, there are restrictions on the combinations of turns that may be used.

By allowing "floating" coupling loops, both of the above disadvantages are overcome. In the circuit of Fig. 13, the turns N , N_1 , and N_2 are completely inde-

pendent. The case $N_1=N_2$ is equivalent to the maximum range case $N'=2$, $N_B'=1$ in the inner leg drive case, which in turn is equivalent to the maximum range case $N=4$, $N_B=1$ for compatible bias. The equations for this case are identical to the equations for compatible bias if N is replaced by $2(N_1+N_2)$ and N_B is replaced by N_1 .

Note that with $N_1=N_2$ and with I_A^{\max} applied, the circuit of Fig. 13 exactly matches the conditions of Fig. 6(d), except that in this case the stress on the outer leg of the transmitter (and receiver) is applied directly from a drive winding instead of from coupling loop current. Current flows in the coupling loop only during *one* transfer.

V. COUPLING LOOP FLUX RELATIONS

The principal quantities of concern in these circuits are flux and current. Data are stored in particular flux patterns, and the currents are provided to move these patterns about in appropriate manner. In the earlier sections of this paper, it was implicitly assumed that the necessary flux relations were taken care of separately and that a reasonable estimate of range could be obtained by supposing that no flux switches during *zero* transfer and that complete switching occurs during *one* transfer.

In order for stable two-level operation to exist, the input (or received) flux ϕ_R at each transfer and the input flux ϕ_R' at the previous transfer must be related as indicated in Fig. 14, where the gain $G=\phi_R/\phi_R'$ is >1 in the interval $\phi_I < \phi_R' < \phi_U$ and is <1 in the interval $\phi_L < \phi_R' < \phi_I$. Thus, the transfer operation will tend to increase a "low" *one* level of flux toward ϕ_U , and to decrease a "high" *zero* level of flux toward ϕ_L . This is equivalent to saying that with such a gain relation, the operation stably protects against "zero build-up" and "one build-down."

With turns ratio greater than unity, *i.e.*, $N_T > N_R$, it is a straightforward matter to arrange a coupling loop to obtain the necessary relation between ϕ_R' and ϕ_R . Suppose that there are no losses in the coupling loop of Fig. 15(a). Then by integrating the relation $N_T \phi_T = N_R \phi_R$, which must hold at every instant of the switching period, we find the relation $N_T \phi_T = N_R \phi_R$, where ϕ_T and ϕ_R are the net flux changes in the transmitter and receiver. Then, provided $\phi_T = \phi_R'$,

$$\frac{\phi_R}{\phi_R'} = \frac{N_T}{N_R} > 1.$$

This relation between ϕ_R and ϕ_T is illustrated in Fig. 15(b). Notice that the linear relation holds only until ϕ_R saturates. In order finally to obtain the necessary relation of Fig. 14(b), consider the coupling loop of Fig. 15(c) in which a "clipper" core is added. This core is arranged to have a total flux linkage capacity of ϕ_C , which is a relatively small fraction of the saturation flux of the MAD's. However, the switching threshold is much

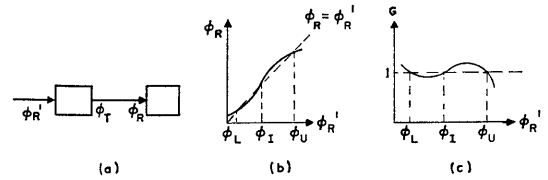


Fig. 14—Gain relations for bi-stable operation.

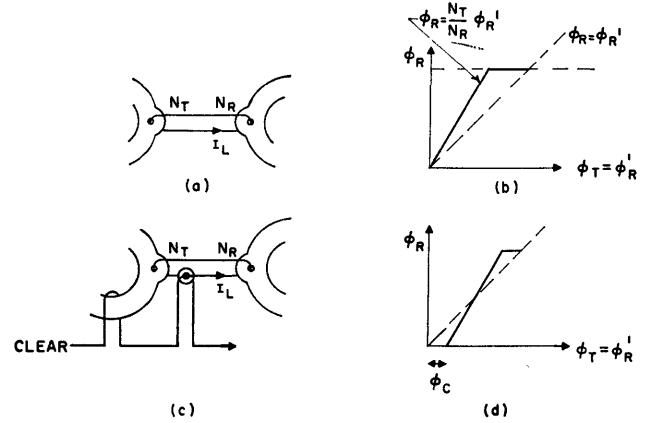


Fig. 15—Coupling loop arrangement for achieving proper gain relations.

lower than that of the receiver, and therefore, its full capacity of flux will be substantially switched before the receiver begins switching at all. In this way, a constant amount of flux is subtracted from the quantity $(N_T/N_R)\phi_T$ when $>\phi_C$; if $(N_T/N_R)\phi_T < \phi_C$, then $\phi_R = 0$. The resulting relation between ϕ_R and $\phi_T = \phi_R'$ is shown in Fig. 15(d). Notice that this curve has the proper form for bistable operation (with $\phi_L = 0$ in this case). If the flux clipper is cleared at the same time as the transmitter, none of the basic clock cycle operations of Fig. 4 is altered, and very good transfer loop operation is achieved.

The use of a flux clipper along with the condition $N_T/N_R > 1$ makes the gain properties of the transfer loop very explicit. However, a flux clipper is not actually required. In fact, it is further demonstrated in the following sections that the relation $N_T/N_R > 1$ is also not required and that successful operation can be achieved with $N_T/N_R \gtrsim 1$. The case $N_T = N_R$ is interesting because the transfer loop is symmetrical, and bi-directional shifting is possible by merely reversing the sequence of Clear pulses or sequence of Advance pulses in Fig. 4. The case $N_T = N_R = 1$ is particularly interesting because of the simple assembly schemes that are made possible. The case $N_T > N_R$ is useful where bi-directional properties are not necessary, and extra flux gain is required. No particular advantages can be seen for the case $N_T < N_R$.

An explicit clipper core is not required because a partial clipping action is performed by the parasitic resistance and inductance of the coupling loop. With the Advance current set in the middle of its range, neither the transmitter nor receiver is brought up to its thresh-

old level during *zero* transmission. Thus, during *one* transmission, a considerable amount of current must be steered to the receiver before any flux can be switched there at all. As the current begins to rise, flux linkage is lost (or stored) in the loop inductance L in the form of LI_L volt-sec, where I_L is the loop current. Any of this stored flux linkage remaining in the loop after switching stops in the receiver (whether due to the advance pulse ending or to the receiver current dropping below the effective threshold) is dissipated in the loop resistance and lost. Furthermore, there is an additional resistive loss of flux linkage in terms of $\int I_L R_L dt$ (where I_L and R_L are loop current and resistance) during the time in which the receiver is switching. Most significantly, however, for sufficiently low levels of flux, ϕ_T will be absorbed entirely into $\int I_L R_L dt + LI_L$ before I_L brings the receiver up to threshold, and therefore ϕ_T will be 100 per cent lost. Hence the plot of ϕ_R vs ϕ_T will start from zero at some value of $\phi_T > 0$, just as in Fig. 15(d).

Unlike Fig. 15(d), the curve will now not be linear, but as long as the turns ratio is just great enough to bring the curve above the $\phi_R = \phi_R'$ line at some higher value of ϕ_R' , bistable operation will be achieved. The turns ratio required is not high, 6/5 being a typical example. In fact, a high turns ratio is quite undesirable, since the excess drive available for switching is reduced. For example, if $N_T/N_R = 2$, then for a simple coupling loop with no bias, $I_{T0} = F_2/N_T$ is an upper bound on the current available for steering to the receiver during *one* transfer. The receiver mmf provided by this current would be $(N_R/N_T)F_2 = (1/2)F_2$, whereas the corresponding figure for unity turns ratio would be F_2 .

Before discussing the properties of unity-turns-ratio operation ($N_T = N_R$), let us consider some basic switching properties of magnetic cores that will be useful in later discussions.

VI. SOME BASIC SWITCHING PROPERTIES OF CONVENTIONAL CORES

Consider the flux-current relations for the conventional toroid of Fig. 16(a). Assume that the B - H curve for the material is ideally square, Fig. 16(b).

With very long setting pulses I_s , the ϕ_s - F_s curve is as indicated in Fig. 16(c), where ϕ_s is the amount of switched flux in response to a setting mmf $F_s = N_s I_s$ applied to a well-cleared core. The ratio F_b to F_a is the same as the ratio r_o to r_i (outer to inner radius). This curve may be automatically plotted by setting up a continuous pattern of alternate Clear and Set currents, in which the Set current is made to vary in amplitude from cycle to cycle. By deflection of an oscilloscope beam in the x direction in response to current I_s and in the y direction in response to switched flux ($= \int edt$), the ϕ_s - F_s curve is automatically traced. In all of the ϕ - F curves to be considered here, ϕ represents remanent flux (*i.e.*, does not include the elastic or reversible component of flux). To plot remanent flux curves, it is only necessary to energize the oscilloscope beam just after

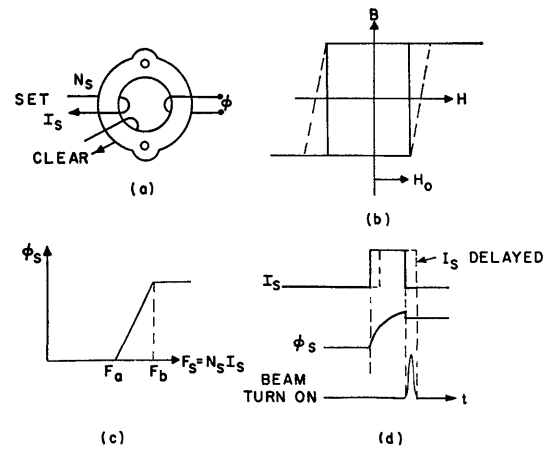


Fig. 16—Core switching experiment.

the setting current is over, by which time the elastic flux has been removed. To maintain the x deflection unchanged until such a time as the beam is energized, it is merely necessary to connect the Advance current pulse to the x deflection plates via a delay line, Fig. 16(d).

An interesting property to consider in relation to the ϕ_s - F_s curve is its dependence on the pulse width of the setting current. Consider a switching model in which it is assumed that the switching rate dB/dt in any portion of the material is proportional to the instantaneous excess drive $(H - H_0)$, where H_0 represents the threshold field. Although idealized, this model does result in the usual inverse relationship between switching time and excess field for the case of a thin ring of material. By its use, calculated ϕ_s - F_s curves for different pulse widths are shown in Fig. 17(a). For very long pulse widths (*i.e.*, $T \rightarrow \infty$), the curve reduces to that shown in Fig. 16(c). However, for a given drive F , as T decreases, a smaller and smaller amount of flux is switched; hence the ϕ_s - F_s curves are monotonically lowered as T decreases. With this model, for pulse widths greater than some critical value T_c , each curve has a linear region marked on the lower end by the mmf required to just saturate the inner radius in time T , and on the upper end by the mmf required to just start switching the material at the outer radius. The nonlinear connecting regions are approximately parabolic for relatively thin-walled cores having a ratio of outer to inner radii of about 1.3 or less.²

In Fig. 17(b) is shown an actual family of ϕ_s - F_s curves. For later comparison, these and all later curves, unless otherwise stated, are taken on an experimentally molded MAD element (having the nominal dimensions indicated in Fig. 19) treated as a conventional core. By

² It may also be noted that these curves have the identical form as for the case in which a very long switching pulse is used on a core having the same dimensions as here but for which the slope of the "rising" portion of the B - H curve of the material is a variable. With truly vertical sides, the curve $T \rightarrow \infty$ applies. With the sides less steep, as shown by dotted lines in Fig. 16(b), the family of ϕ_s - F_s curves has the identical form of Fig. 17(a).

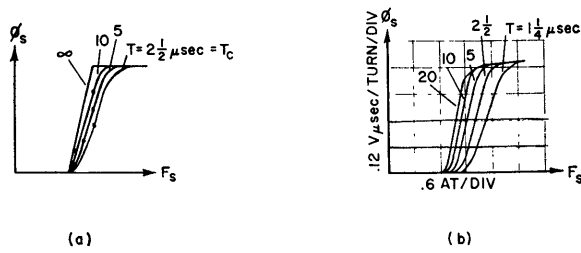


Fig. 17—Calculated and measured ϕ_s - F_s curves.

shaping about the apertures as indicated in Fig. 19, the results are substantially identical with results obtained on actual toroids of the same material. Notice that, compared with the curves of Fig. 17(a), these curves do not radiate in so pronounced a fashion from the value F_a , but rather are mainly translated horizontally to higher values of mmf as the pulse length decreases. This property is very important in MAD elements for reasons that will become clearer below.

If one looks at the corresponding switching voltage curves for this element, it becomes apparent what is causing this translation of the ϕ_s - F_s curves. This family of voltage curves vs time is indicated in Fig. 18, where the parameter is the magnitude of I_s (where I_s is a very long pulse). The curves of Fig. 18(a) are calculated using the model $dB/dt \propto (H - H_0)$. Notice that this simple model is very inadequate for predicting the front end of the voltage curves. This fact is understandable, since this model relates more to the rate of movement of existing domain walls. However, if we start with a well-cleared core in which there is a minimum of reverse domains (walls), then after the pulse I_s is turned on, it takes a time for domain walls to be established.³ This is reflected in the initial slope of the voltage curves. In any case, notice the difference in behavior of the peaks of the voltage curves as a function of I_s . In the family of actual curves, there is a large "peaking delay" at low levels of switching. With materials that exhibit significant peaking delay properties, the voltage is almost exactly zero before the time of peaking. It is straightforward to convert the voltage curves of Fig. 18(b) into the ϕ_s - F_s curves of Fig. 17(b) and see the reason for the increase in threshold of the narrow-pulse curves with peaking delay.

It may be noted that peaking delay is a property of some materials and not others. For example, there are materials for which the peaks in the switching curves of Fig. 18(b) lie almost directly over each other. For these materials, the ϕ_s - F_s curves are more like those of Fig. 17(a).

Given a core of appropriate material, it is further necessary, in order for the core to exhibit peaking delay, that the setting current I_s be applied to a well-cleared core. Generally speaking, Clear strengths of at

³ N. Menyuk and J. B. Goodenough, "Magnetic materials for digital computers, I. A theory of flux reversal in polycrystalline ferromagnetics," *J. Appl. Phys.*, vol. 6, pp. 8-18; January, 1955.

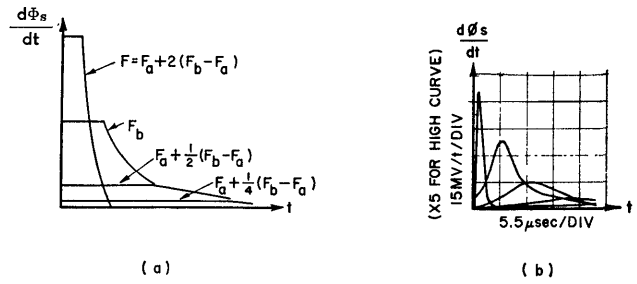


Fig. 18—Calculated and measured $d\phi_s/dt$ -time curves.

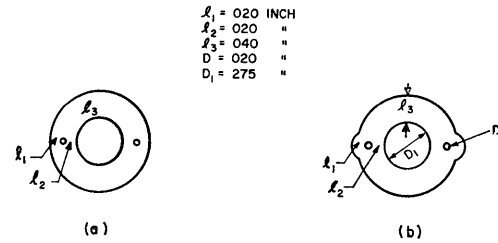


Fig. 19—Shaping of MAD elements.

least two to three times threshold are required for good peaking delay.

If a MAD is made by cutting apertures in the wall of a conventional toroid, Fig. 19(a), then regardless of the Clear magnitude, it is impossible to get all material on a major loop since the cross-sectional area $1_1 + 1_2$ is less than 1_3 for a core of unit height. Thus, even for material that is potentially capable of exhibiting peaking delay, this type of construction nullifies the effect. However, by appropriate shaping of the element, e.g., so that $1_1 + 1_2 = 1_3$, the element treated as a simple toroid will exhibit significant peaking delay.

Another very important switching property related to peaking delay is shown by the families of ϕ_s - F_s curves taken for the condition in which the core is preset before I_s is applied. The families of ϕ_s - F_s curves shown in Fig. 20, contain the magnitude of preset flux ϕ_p as the parameter. The difference between the various families of curves are that they are taken for different combinations of long and short duration preset and set pulses.

For zero preset ($\phi_p = 0$), the total switched flux ϕ_s is $\phi_s^{\max} = \phi^M$, where ϕ^M represents the total flux capacity of the core from saturation in one direction to saturation in the other. When a core has been preset, the current I_s has correspondingly less flux available to switch. Thus in Fig. 20(b), as the amount of preset flux ϕ_p increases, the maximum switchable flux $\phi_s^{\max} = \phi^M - \phi_p$. For tracing these curves automatically, a repeating cycle of Clear, Preset, and Set currents is applied to the core of Fig. 20(a).

For each curve, the Preset current is adjusted to the appropriate level and the Set current is made to vary from cycle to cycle. The oscilloscope plotting is exactly as indicated in connection with Fig. 16(d), where the beam is turned on just after the Set current is over.

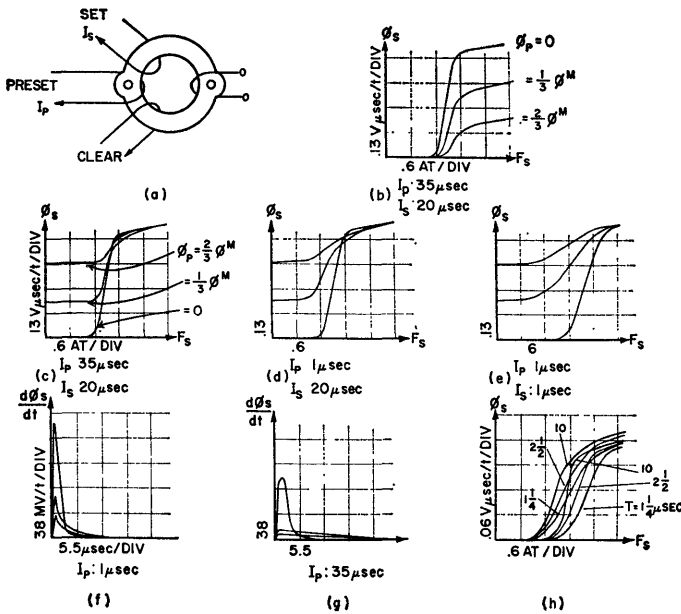


Fig. 20— $\phi_s - F_s$ and $d\phi_s/dt$ -time curves for various pulse lengths of I_p and I_s .

For later convenience in dealing with families of curves for MAD elements, the curves of Fig. 20(b) are redrawn in Fig. 20(c) with the final rather than initial values of flux superimposed. Actually, this is equivalent to raising the zero flux level for each curve by the magnitude ϕ_p .

When a well-cleared core is preset to a certain level of flux by a long current pulse, one can visualize the flux condition in the core to be represented by a circumferential domain wall outside of which the flux is in a clockwise (Clear) direction and inside in a counterclockwise direction. Except in the transition region, substantially all material is well saturated. Since I_s stresses the core in the same direction as I_p , it is reasonable for gentle preset (long pulse) that, regardless of preset level, the current I_s should continue the switching where I_p left off, and with essentially the same threshold, as demonstrated in Fig. 20(c). Let us now consider the effect of shortening the pulse durations. In order for a certain magnitude of flux, ϕ_p , to be preset as the preset pulse is decreased in length, the magnitude of the preset current must be increased. For significant decrease in duration, the magnitude of current must be likewise considerably increased. For a reasonably thin-walled core, this increased magnitude of current is capable of switching flux simultaneously throughout the entire core, so that the current pulse must be shut off when the proper level of preset flux is reached. In this case, it is certain that reverse domains are distributed throughout the body of the core in some random fashion. Thus it is hardly surprising that after such a preset pulse, the set current, which tends to continue the switching in the same direction, finds a much lower and less abrupt threshold. This effect is clearly seen when the curves of Fig. 20(c) and 20(d) are compared.

Let us next consider the effect of short set and preset pulses, Fig. 20(e). For $\phi_p = 0$, the $\phi_s - I_s$ curve is just the appropriate curve of the family of Fig. 17(b), for the given pulse duration. If we compare the curves of Fig. 20(d) and Fig. 20(e), we notice that in the latter case, the threshold moves a considerable distance to the right for zero preset, but not quite so far for nonzero preset. This is reasonable in terms of the previous discussion of the effects of a good Clear state on peaking delay. Good peaking delay occurs only when all of the material is in a well saturated condition. However, due to presetting with a short pulse, a random distribution of reverse domains is left throughout the core, resulting in very poor peaking delay after preset and hence very little increase in threshold for a short-pulse set. This point is demonstrated by the voltage-time curves (similar to those of Fig. 18) taken after a preset condition of $\phi_p = 1/2 \phi^M$ using a short preset pulse, Fig. 20(f), and a long preset pulse, Fig. 20(g). Notice the significant difference in switching times for these two families. The effect of preset is also demonstrated in the $\phi_s - F_s$ curves, Fig. 20(h), taken for the same preset level $1/2 \phi^M$. The group of curves radiating from the lower threshold value of F_s is for the short preset pulse; the other group is for the long preset pulse. The lowering of threshold for short preset pulses is clearly seen. Within each group, the parameter is the duration of Set pulse.

VII. SWITCHING PROPERTIES OF MAD'S

Ideal Family of Output Curves

In Fig. 1, output $\phi_T - F_T$ curves were shown for the two cases of a Set and Clear MAD. Actually, there exists a whole family of such curves with the amount of preset (or input) flux as the parameter (Fig. 21). In Fig. 21(a), the input current is shown linking leg l_1 about the input aperture, and the output current is shown linking leg l_4 about the output aperture. Assume all legs are of equal dimension. Let ϕ^M represent the total flux capacity in any leg from saturation in one direction to saturation in the other direction. With leg l_4 saturated in the Clear (clockwise) direction, application of I_T of sufficient magnitude will switch an amount of flux ϕ^M in leg l_4 independent of the amount of preset flux. A portion of it equal to $\phi_p (= \phi_{in})$ will switch locally about the output aperture and the remainder will switch around the main aperture. If all material is operating on an ideal rectangular hysteresis loop, the family of curves will have the form indicated in Fig. 21(b).

Actual Family of Output Curves

Actual families of output curves, for the same MAD used for the above tests of core switching properties, are shown in Fig. 22. These curves are automatically plotted by the method previously described and are taken for the same combinations of long and short current pulses indicated in Fig. 20. Notice that the effects are substantially the same as observed in the case of presetting

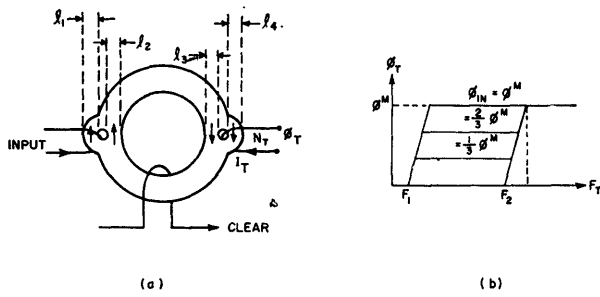


Fig. 21—Idealized family of output curves ϕ_T - F_T for a MAD.

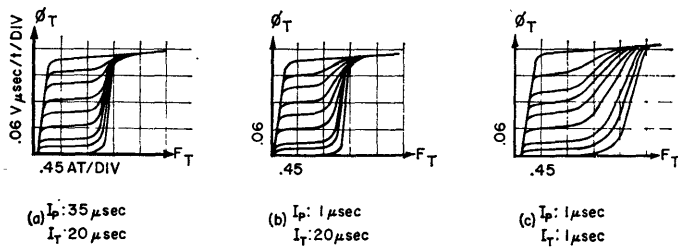


Fig. 22—Actual families of ϕ_T - F_T curves for various input and output current pulse durations.

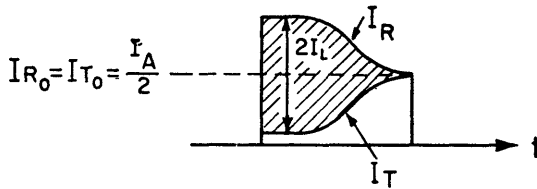


Fig. 23—Transmitter and receiver currents during one transfer.

a toroid. Actually, the short-short current pulse combination is the one of interest, because this more nearly approximates actual operation. In Sections III and IV, it was indicated that in biased circuits, the transmitter and receiver are switched with two or more thresholds of current. This operation corresponds to high-drive, short-pulse conditions of measurement. However, it is shown below that for one transfer, the transmitter current I_T and receiver current I_R are not constant in time. To this extent, the above experimental families of curves, which are plotted for rectangular input and output current pulses, do not apply. Nevertheless, they are extremely indicative of the nature of the operation.

The main significance of these curves is the lowering of the main aperture threshold for partial set levels relative to the Clear State threshold. It is demonstrated below that this property provides a mechanism for obtaining proper gain relations for unity-turns-ratio operation.

Transmitter and Receiver Currents

In the (ideal) zero transfer case, assuming unity turns ratio, the Advance current I_A divides into equal branch currents $I_{T_0} = I_{R_0} = (1/2)I_A$, where the sub "0" stands for the zero case.

During a one transfer, the Advance current divides

into unequal branch currents I_T, I_R such that at all instants of time $\phi_T = \phi_R$. Because of the lower threshold (neglecting the voltage drop in the loop resistance and inductance) in the transmitter, $I_R > I_T$, but always $I_R + I_T = I_A$. This situation can be characterized by a loop current I_L superimposed on the zero transfer currents so that $I_R = I_{R_0} + I_L$ and $I_T = I_{T_0} - I_L$

$$\left(\text{where } I_{R_0} = I_{T_0} = \frac{I_A}{2} \right), \text{ or } I_L = \frac{I_R - I_T}{2} .$$

During one transfer, the transmitter may be characterized as a relatively small, thick-walled core [see e.g., Figs. 9(b) and 10(b)] compared with the receiver. Thus, for given magnitudes of I_T and I_R [assuming the switching model $dB/dt \propto (H - H_0)$], the ratio of switching rates at the outer and inner walls is much higher in the transmitter than in the receiver. For constant I_T and I_R , the rates of flux change $\dot{\phi}_T$ and $\dot{\phi}_R$ will be constant in time only as long as no material saturates. Clearly, the inner wall of the transmitter will saturate first. When this happens, $\dot{\phi}_T$ tends to decrease, since less material participates in the switching. However, this tendency is counteracted by an increase of I_T to bolster up $\dot{\phi}_T$ at the expense of $\dot{\phi}_R$ (i.e., I_R decreases), so that at all times the relation $\dot{\phi}_T = \dot{\phi}_R$ is maintained. Thus, the resulting I_T and I_R curves have the general form indicated in Fig. 23.

The main significance of the current relations indicated here is that during one transfer, the transmitter current is initially low but rises toward $I_A/2$ while transfer continues.

The ϕ^* Contribution to Flux Gain

Flux gain G from one stage to the next may be defined as $\phi_R/\phi_{R'}$ where $\phi_{R'}$ is the flux received in the transmitter during the previous Advance pulse. If during the present Advance pulse, all available flux about the output aperture is switched but none is switched about the main aperture of the transmitter, then $\phi_T = \phi_{R'}$. Now $\phi_R = \phi_T - \phi_{\text{loss}}$, for a single-turn coupling loop (a special case of unity-turns-ratio operation) where ϕ_{loss} , the flux loss in the loop resistance R_L , is $\int I_L R_L dt$ volt-sec. Hence, if $\phi_T = \phi_{R'}$,

$$G = 1 - \frac{\phi_{\text{loss}}}{\phi_{R'}} .$$

Note that $G > 1$ is impossible here because of the subtractive loss term. This equation is characteristic of the operation of a conventional core-diode-type shift register, which requires $N_T > N_R$ in order to obtain $G > 1$.

In a MAD arrangement, ϕ_T can be more than $\phi_{R'}$ because of the possibility of flux switching not only locally about the output aperture, but also around the main aperture in a direction to increase the setting of the element. For illustration, assume that the Advance current is set in the center of its range, or $I_A = I_A^{\text{av}}$, so that $NI_A/2$ is below threshold F_2 as indicated in Fig. 24. Also

assume a level of input flux $\phi_{R'}$ as indicated in the figure. Then as I_T increases from its initial low level (see previous section) towards its steady-state value $I_A/2$, it soon enters a region in which flux may be switched about the main aperture. This flux is defined as ϕ^* . Thus $\phi_T = \phi_{R'} + \phi^*$ and the gain equation is modified to read

$$G = 1 + \frac{\phi^*}{\phi_{R'}} - \frac{\phi_{\text{loss}}}{\phi_{R'}}.$$

It is clear from Fig. 24 that ϕ^* is a function of $\phi_{R'}$ having the form indicated in Fig. 25. ϕ^* is very small at low levels of received flux because the maximum value of NI_T is below threshold for switching around the main aperture. ϕ^* is also very small for large $\phi_{R'}$ because of saturation. It is important to note that because of the finite slope of the ϕ_T - F_T curve below threshold (even for the Clear state curve) that ϕ^* is everywhere >0 , and hence that $\phi^*/\phi_{R'} \rightarrow \infty$ as $\phi_{R'} \rightarrow 0$. Thus the contribution of the term $\phi^*/\phi_{R'}$ to the gain equation has the form indicated in Fig. 25(b). The steeply rising portion of this curve for low values of $\phi_{R'}$ contributes to the lower unity-gain crossing of the Gain- $\phi_{R'}$ curve at $\phi_{R'} > 0$, resulting in $\phi_L > 0$, as would be expected. Thus, if over some interval, the ϕ_{loss} term is smaller in magnitude than the ϕ^* term (for $\phi_{R'} > \phi_L$), then a gain curve of the form indicated in Fig. 14 can be obtained, and the interval in question is just the interval $\phi_I < \phi_{R'} < \phi_U$ where $G > 1$.

Resistive Flux Loss

The resistive flux loss, $\int I_L R_L dt$, is just proportional to the cross-hatched area in Fig. 23. An accurate analysis of ϕ_{loss} is extremely difficult, since no accurate switching model is available for predicting the current shape $I_L(t)$ as a function of flux level, $\phi_{R'}$.

In Sections II to IV, for purposes of comparing switching speeds for various circuit arrangements, it was assumed that I_A divides into I_T and I_R in such a way as to apply equal multiples of threshold mmf to transmitter and receiver. This model does result in the correct ordering of the different circuits in terms of speed, but it is very inadequate for predicting $\phi_{\text{loss}}/\phi_{R'}$ as a function of $\phi_{R'}$ for a given circuit. This fact should be quite obvious just from the complexity of measured switching characteristics as represented in Figs. 20 and 22.

True, one can definitely say that ϕ_{loss} increases with $\phi_{R'}$, but not even this much can be said about the ratio $\phi_{\text{loss}}/\phi_{R'}$, except for very low values of $\phi_{R'}$. In this latter case, as was indicated earlier in the discussion of the partial clipping action of loop inductance and resistance, $\phi_{\text{loss}}/\phi_{R'}$ will be essentially unity for sufficiently low flux levels.

In effect, then, all that can be said at present is that the loss term will decrease from near unity for very low $\phi_{R'}$ to a value Δ at some low $\phi_{R'} (= \phi_1)$ and remain below

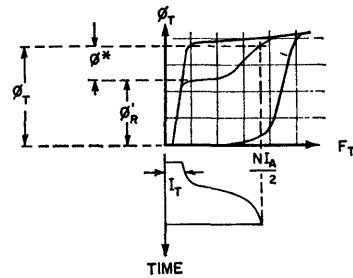


Fig. 24—Demonstration of ϕ^* flux gain.

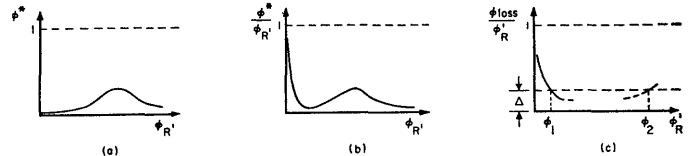


Fig. 25—Plot $\phi^* - \phi_{R'}$, $\phi^*/\phi_{R'} - \phi_{R'}$ and $\phi_{\text{loss}}/\phi_{R'} - \phi_{R'}$.

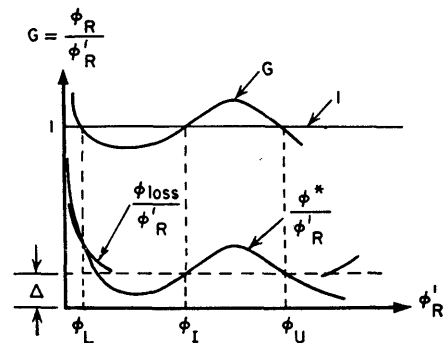


Fig. 26—Addition of gain equation components to form the gain curve.

Δ at least up to some high $\phi_{R'} (= \phi_2)$, as indicated in Fig. 25(c).

In Fig. 26, it is shown how the three terms of the gain equation

$$G = 1 + \frac{\phi^*}{\phi_{R'}} - \frac{\phi_{\text{loss}}}{\phi_{R'}}$$

may add to give the required form indicated in Fig. 14. The loss term is added as though equal to Δ in the indeterminate interval $\phi_1 < \phi_{R'} < \phi_2$.

Whatever the actual variation of the loss term in this interval, then, the qualitative nature of the gain curve will not be changed, rather only the locations of the unity gain points ϕ_I and ϕ_U .

Flux Boost

In order to get reasonable Advance current range, the short-short ϕ_T - F_T curves [Fig. 22(c)] should have the Clear state curve moved as far to the right as possible, and the higher level flux input curves moved as far to the left as possible. Experimental results have indicated that these conditions are generally met best by

materials exhibiting good peaking delay properties [Fig. 18(b)].

The range analysis of Sections II to IV does not apply well to the unity-turns ratio case since the advance current is more limited by the requirement of getting ϕ^* to make up for flux losses than by the assumptions of Section II.

In any case, the situation can be significantly improved by the circuit described here.

Between the time that the flux ϕ_R is received, and flux ϕ_T is transmitted to the next stage, the previous element is cleared. By having this pulse do double duty, as indicated in Fig. 27, the flux boost may be obtained (at Clear time) before transfer out of the element occurs. With N turns on the receiver, the Clear current is adjusted so that the receiver is brought up to the vicinity of threshold F_2 . Thus, if ϕ_R is low (as for a zero), then the boost pulse has essentially no effect. If ϕ_R is high (as for a one) but less than ϕ^M because of ϕ_{loss} during transmission, then the boost pulse will increase the set level of the element.

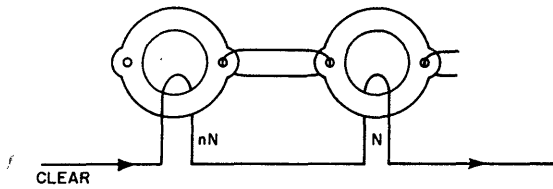


Fig. 27—Circuit for achieving flux boost.

The family of curves of Fig. 24 is taken with a winding about the output aperture. However, the reduced thresholds for partially set levels are characteristic of the state of the entire element (as previously described) and would also be observed in ϕ - F curves taken on the flux boost winding. Thus the effect of the flux boost current can be predicted from the ϕ_T - F_T curves.

The Clear winding has nN turns, which results in the transmitter being cleared with n thresholds of mmf. For good clearing, n should be greater than 2. By consulting Fig. 4, we see that with this new arrangement, two processes are going on simultaneously in the receiver. Clearing the transmitter causes a negative set current to switch flux locally about the input aperture of the receiver, and the mmf applied by the flux boost winding causes additional set flux to be switched about the main aperture.

In all previous circuits, the Clear pulse had unlimited range as long as it was above some minimum. Such is not the case in the present circuit, since the Clear current works against a threshold. However, although the Clear current range is decreased, the Advance range is significantly increased.

The flux boost method of making up flux losses has three main advantages compared to the ϕ^* method.

First, there are no coupling-loop losses associated with flux boost, whereas part of the available ϕ^* is always lost during transfer. In fact, with flux boost, it is possible for the receiver to be set fully before flux is transferred out of it; this condition is impossible to obtain for unity-turns-ratio operation without flux boost, because of losses. Second, the boost current has a fixed magnitude and duration independent of flux level, whereas the current I_T switching ϕ^* is greater (at least in integrated value) for low flux levels than for high levels. Third, the boost current can be adjusted in width and amplitude independently of the advance current, while the mmf that switches ϕ^* is tied to the advance current.

It is pertinent to note that with flux boost taking care of the flux-gain requirement, Advance range is more closely predicted by the relations of Sections III and IV. Furthermore, flux boost may be used advantageously in connection with all of the circuits derived in that section. This is so in particular for unity-turns-ratio operation, but advantage can be obtained even for circuits in which $N_T/N_R > 1$.

VIII. RESULTS AND CONCLUSION

The range and speed relations derived in Sections III and IV, although based on a very simple model, do properly predict comparative results for the various circuit arrangements. As pointed out in the discussion on flux boost, these relations do not apply well for unity-turns-ratio circuits if flux boost is not used. In this case, the Advance currents must be adjusted more to satisfy the flux gain requirements than the simple switching model used to derive these range and speed relations. Listed below is an example of the types of comparative results obtained with a coupling loop using $N_T = 6$, $N_R = 5$, for the circuits indicated.

Circuit of Fig.	Bias turns $N_{BT} = N_{BR}$	Range
5	—	15 per cent
10	1	30 per cent
11	2	50 per cent, using 50 per cent dc counter bias

Flux boost helps even where $N_T > N_R$. For example, when flux boost is used, the 15 per cent range obtained using no bias will increase to about 30 per cent. In flux boost circuits in general, the Clear and Advance currents may be independently adjusted to give either one a high range at the expense of the other. The range value given here, however, implies that the Clear and Advance currents are adjusted so that they both have the same range, namely 30 per cent.

Unity-turns-ratio coupling loops, *i.e.*, with $N_T = N_R$, have operated with the following typical results. With the bias circuit of Fig. 10, $N = 4$, $N_B = 1$, and flux boost, Clear and Advance ranges of greater than 40 per cent each are achieved. These results are obtained with 1- μ sec

Clear and Advance pulses driving a register of experimentally molded elements having the dimensions indicated in Fig. 19 and made with material having a long-pulse threshold of 0.7 oersted. Single-turn coupling-loop circuits with the same effective bias operate equally well.

The detailed analysis of these circuits is difficult not only because of the usual difficulties of dealing with the dynamic properties of highly nonlinear elements, but also because of the relatively complex geometries involved. It is clear that a good deal of the design of these circuits is necessarily based on intuition and empirical results. The circuits described here can be made to operate quite well, however, and the lack of analytical

tools is felt more in trying to decide how or when a particular arrangement is optimum. It is hoped that future efforts will result in the development of satisfactory switching models that will make the circuit design procedure routine.

The techniques presented here provide the potential for developing extremely reliable digital circuitry at least for the intermediate computer speed ranges of 0.1 mc to 1 mc clock (or bit) rates.

IX. ACKNOWLEDGMENT

The authors wish to acknowledge the very helpful suggestions and contributions of their colleague, Dr. Douglas Engelbart, to the material presented here.

A Twistor Matrix Memory for Semipermanent Information*

DUNCAN H. LOONEY†

INTRODUCTION

A NEW magnetic matrix memory has been developed for the storage of semipermanent digital information. The memory is designed for computers which require random access to stored information that is changed very infrequently. The information is stored in a pattern of permanent magnets arranged on a plastic board. The presence or absence of a permanent magnet is sensed nondestructively by a wire wrapped with a magnetic tape placed close to the permanent magnet. A stored word is read by a linear selection system using a biased core access switch.¹

The memory is fabricated in modules. A typical module is shown in Fig. 1. The photograph shows a 512-word memory consisting of 32×16 word locations. Each word location stores 26 bits of information. Any word location in the memory may be selected at random and the information read in a period of a few microseconds. The temperature range of operation of the memory is extremely wide.

The concept of storing information in an array of permanent magnets was advanced by the late S. Shackell. Mr. Shackell's work was interrupted by his untimely death and has not been previously reported in the

literature. With the development of the twistor,² John Janik, who was familiar with the Shackell scheme, suggested its use in such a system to reduce the size of the permanent magnets.

The operation of a store using the 512-word memory module is described in a companion paper.³ The store, which utilizes all solid-state circuitry, is compared to other systems using photographic or magnetic techniques which can be used for the storage of semipermanent information.

OPERATING PRINCIPLE

The information is stored in an array of small permanent magnets. The presence of the magnet is sensed by a wire wrapped with magnetic tape placed close to the magnets. A group of 26 wrapped wires are encapsulated in a plastic tape. The encapsulated wires are then enclosed in a set of copper solenoids as illustrated in Fig. 2. A particular solenoid corresponding to a stored word may be selected by activating one core of the biased core access switch. The bar magnets are arranged in a pattern on the surface of a thin plastic card. Each magnet is located at the intersection of a wrapped wire or twistor and a solenoid. The purpose of the permanent magnet is to inhibit locally the drive field of

* The work reported in this paper was done for the U. S. Dept. of Defense under Contract DA-30-069-ORD-1955.

† Bell Telephone Labs., Murray Hill, N. J.

¹ J. A. Rajchman, "A myriabit magnetic core matrix memory," *Proc. IRE*, vol. 41, pp. 1407-1421; October, 1953.

² A. H. Bobeck, "A new storage element suitable for large sized memory arrays—the twistor," *Bell Sys. Tech. J.*, vol. 36, pp. 1319-1340; November, 1957.

³ J. J. DeBuske, J. Janik, and B. H. Simons, "A card changeable nondestructive readout twistor store," this issue, pp. 41-46.